Published in final edited form as:
Nat Clim Chang. 2021 February 1; 11: 143–151. doi:10.1038/s41558-020-00963-x.

Zonally contrasting shifts of the tropical rainbelt in response to climate change

Antonios Mamalakis[1,*], **James T. Randerson**[2], **Jin-Yi Yu**[2], **Michael S. Pritchard**[2], **Gudrun Magnusdottir**[2], **Padhraic Smyth**[3,4], **Paul A. Levine**[2], **Sungduk Yu**[5], **Efi Foufoula-Georgiou**[1,2,*]

[1]Department of Civil and Environmental Engineering, University of California, Irvine

[2]Department of Earth System Science, University of California, Irvine

[3]Department of Computer Science, University of California, Irvine

[4]Department of Statistics, University of California, Irvine

[5]Department of Geology and Geophysics, Yale University, New Haven, Connecticut

Abstract

Future changes in the position of the intertropical convergence zone (ITCZ; a narrow band of heavy precipitation in the tropics) with climate change could affect the livelihood and food security of billions of people. Although models predict a future narrowing of the ITCZ, uncertainties remain large regarding its future position, with most past work focusing on zonal-mean shifts. Here we use projections from 27 state-of-the-art (CMIP6) climate models and document a robust zonally-varying ITCZ response to the SSP3-7.0 scenario by 2100, with a northward shift over eastern Africa and the Indian Ocean, and a southward shift in the eastern Pacific and Atlantic Oceans. The zonally-varying response is consistent with changes in the divergent atmospheric energy transport, and sector-mean shifts of the energy flux equator. Our analysis provides insight about mechanisms influencing the future position of the tropical rainbelt, and may allow for more robust projections of climate change impacts.

The intertropical convergence zone (ITCZ) and its dynamics[1] play a vital role in the tropical atmospheric circulation and hydroclimate, sustaining tropical forest and savanna ecosystems, and influencing the livelihoods of billions of people. As such, intense research has focused on identifying the physical mechanisms that determine the climatology and variability of the ITCZ position on intra-seasonal to interannual scales[1-10], and its long-term response to large-scale natural climate variability and anthropogenic forcing[1,5,11-23].

[*]**Corresponding Author:** Correspondence to Efi Foufoula-Georgiou (efi@uci.edu), amamalak@uci.edu.

Author contributions

AM designed the study, performed the data analysis, and wrote the first draft of the manuscript. All authors contributed to the conceptualization and interpretation of the results and to extended discussions in the revising and finalizing stages of the manuscript.

Competing interests

The authors declare no competing financial or non-financial interests.

Past studies have shown that perturbations in the inter-hemispheric asymmetry of the net energy input into the atmosphere will shift the ITCZ toward the more heated hemisphere[1]. For example, projected reductions in aerosol emissions[24-26], arctic sea-ice loss (related to arctic amplification[27,28]) and glacier melting in the Himalayas[29,30] will reduce albedo significantly more in the northern hemisphere than in the southern hemisphere, resulting in northern heating and an ITCZ shift to the north[18,22,31]. In contrast, the Atlantic meridional overturning circulation (AMOC) that is expected to weaken in the future[32-35] (new results indicate that it has already been weakening[36]) will result in a reduction of the northward oceanic heat transport from the tropics to the northern Atlantic and a northern cooling, leading to a southward shift of the ITCZ[22,37,38].

Despite the relative consensus in the literature with regard to the zonal-mean response of the ITCZ location to individual forcing agents as discussed above, there is still high uncertainty regarding the response of the ITCZ location to the integrated effect of all these processes under climate change. This uncertainty mainly stems from different model physics that yield different responses even to identical climate change scenarios. Specifically, although a future narrowing of the ITCZ is a robust projection expected with climate change[20], models differ considerably regarding changes in the position of the ITCZ, yielding to an almost zero zonal-mean ITCZ shift when considering the multi-model mean[22]. Another reason for this uncertainty is that most studies have focused on zonal-mean changes of the ITCZ, possibly masking model agreement over shifts in particular longitudinal sectors. Indeed, because of the compensating effects of the relevant radiative and dynamical processes influencing the ITCZ position, and since most of these processes are not expected to be equally influential in different longitudinal sectors, the integrated ITCZ response to climate change should not be expected to be homogeneous in longitude[18]. Thus, studying the longitudinally-explicit changes of the ITCZ location is necessary to gain insight into its future response and to identify robust model projections across different longitudinal sectors.

Here we explore the ITCZ response to climate change during the 21st century, using 1983-2005 as a base period and comparing with projections during 2075-2100. In our analysis, we use Earth system model simulations from the sixth phase of the Coupled Model Intercomparison Project[39] (CMIP6; a total of 27 different models and 105 indivdual runs; see Supplementary Table 1) forced with the SSP3/RCP7.0 scenario[40,41] (that is, the combination of the shared socioeconomic pathway 3 and the representative concentration pathway 7.0). For each model simulation, we estimate seasonal and annual-mean changes of the ITCZ position as a function of longitude (in 1° increments), while also considering the effect of the models' present-day ITCZ biases on the revealed changes. Given the existing ambiguity in the literature as to a regional ITCZ definition[42], we clarify that for the purposes of this study, the position of the ITCZ is defined as the latitude of maximum (above a specific quantile) precipitation and minimum outgoing longwave radiation (OLR) in each longitude, using a probabilistic approach[43] (see Methods). For the sake of completeness, we also present results based on simpler, univariate precipitation or OLR indices/maps to assess ITCZ changes. We acknowledge that the adopted tracking approaches might be masking inherent differences in regional precipitation features (e.g. land vs oceanic rainbelts), whose however detailed phenomenology and attribution is not the focus in this study.

We provide evidence that models exhibit high consensus regarding future ITCZ shifts as a function of longitude, despite the large inter-model spread in the zonal-mean response. The ITCZ shifts are evaluated for physical consistency with future changes in equatorial sea surface temperature, as well as changes in the atmospheric energy transport and associated shifts in the energy flux equator.

Future zonally contrasting shifts of the ITCZ

The annual and zonal-mean ITCZ shift during the 21st century for the CMIP6 models is −0.5 ± 1.2°N (a small southward shift; see Table 1). The inter-model spread within the CMIP6 models is very large (the standard deviation is more than twice the mean shift), which leads to the multi-model mean shift not being statistically distinguishable from zero, and confirming previous reports[22,44].

Despite the high inter-model uncertainty regarding the zonal-mean ITCZ shift, the CMIP6 models show greater agreement for different longitudinal sectors (see Figure 1 and Methods for information on the tracking approach of the ITCZ; explanatory schematics are provided as Supplementary Figures 1-2). For the May-Oct season, the models exhibit a robust northward shift of the ITCZ over eastern/central Africa and the Indian Ocean, and a southward shift over most of the Pacific and Atlantic Oceans; Figure 1a. The projected shift over Indian Ocean comes primarily from a northward shift in the near-equatorial precipitation (which represents a secondary ITCZ feature in the present-day observations during this season that is physically linked with the so-called “equatorial jump” [45,46]), rather than a shift in the subtropical “monsoonal” primary convergence zone. The revealed shift has been argued to associate with future increases in sea surface temperature in the northern Indian Ocean and locally developed Bjerknes feedbacks between sea surface temperature gradients, and wind and thermocline changes in the basin[47]. In the Nov-Apr season, the south Indian Ocean convergence zone and the south Pacific convergence zone both shift northward[48], while the eastern Pacific ITCZ is shown to shift southward. In the Atlantic basin, there is an equatorward shift of the ITCZ. In general, zonally distinct (and contrasting) responses of the position of the ITCZ to climate change occur during both seasons and an even more robust response is visible on annual time scales (see Figure 1c and Table 1). This response consists of a northward shift over the eastern Africa and Indian Ocean, and a southward shift over the eastern Pacific Ocean, the Atlantic Ocean, as well as the South America (where a less robust southward shift is shown). The zonally distinct responses are also apparent when calculating the future changes in precipitation or OLR (see Supplementary Figures 3-4).

To more precisely quantify the zonally distinct responses of the ITCZ to climate change, we tracked the temporal evolution of the ITCZ location as a function of longitude and over two different longitudinal sectors. We define the Eurasian sector as spanning 20°E-130°E and the eastern Pacific – Atlantic sector as spanning 250°E-360°E. We note that the boundaries of these sectors were chosen from visible breaks shown in Figure 2a, but our results are robust if the boundaries are moderately changed (i.e., by ±10° of longitude). A northward ITCZ shift occurs for the Eurasian sector, while a southward shift occurs in the eastern Pacific – Atlantic sector (Figure 2a). Over the western Pacific, the ITCZ shifts southward during May-

Oct and northward during Nov-Apr (as shown in Figure 1), which translates into a decreased seasonal ITCZ migration in the future, and an annual-mean shift that is nearly zero. When comparing the 2075-2100 and 1983-2005 periods, a statistically significant (using the *t*-test; $p < 0.01$) northward shift on the order of $0.8 \pm 0.6°$ is obtained over the Eurasian sector (see Table 1). In contrast, over the eastern Pacific – Atlantic sector, CMIP6 models indicate a statistically significant southward shift on the order of $0.7 \pm 0.9°$. The future ITCZ shift and the corresponding change in annual-mean tropical precipitation asymmetry (i.e. change in the quantity: Precip $_{0°\text{-}20°\text{N}}$ − Precip $_{0°\text{-}20°\text{S}}$) between 2075-2100 and 1983-2005 are shown for every CMIP6 model in Figure 2b, indicating that the majority of models predict a future increase in precipitation in the northern subtropics relative to the south over the Eurasian sector (red color). The opposite is true for most CMIP6 models over the eastern Pacific – Atlantic sector (blue color). Figure 2b also shows the robustness of the zonally distinct ITCZ responses with respect to using different indicators to assess changes in the ITCZ position; both the precipitation asymmetry and the ITCZ tracking method yield consistent estimates for most CMIP6 models.

To gain insight about the impact of model biases on our interpretation of the future ITCZ shifts, we have calculated the present-day double-ITCZ biases for each model and over each basin, and then regressed the obtained biases with the future ITCZ shifts (see Methods and Supplementary Discussion). We find that the double-ITCZ biases, if anything, are obscuring the full extent of the southward ITCZ shift over the eastern Pacific – Atlantic sector, and thus, our results regarding the zonally contrasting shifts are on the conservative side; see Supplementary Discussion and Supplementary Figures 5-8.

Overall, the agreement between CMIP6 models over these two sectors (Table 1 and Figures 1-2) provides confidence that climate change will lead to contrasting meridional shifts of the ITCZ in the Eurasian and eastern Pacific – Atlantic sectors. As already mentioned, these contrasting responses nearly cancel one another, leading to almost zero ITCZ shift from a zonal-mean perspective (Table 1), confirming the recent literature[22,44].

Regional mechanisms

Motivated by the known close coupling between sea surface temperature (SST) and precipitation in the tropics[47,49,50], we explored the consistency of the revealed zonally contrasting shifts of the ITCZ with changes in SST.

We find that over the tropical Pacific Ocean, SST warming is more pronounced in the east than the west, which is consistent with the anticipated weakening of the Walker circulation with climate change (Figure 3a)[47,51]. In both the eastern Pacific and Atlantic Oceans, higher SST warming occurs at low latitudes between 10°S and 5°N, which is consistent with this region serving as an attractor for a southward shift of the ITCZ from its current baseline position at $4.1 \pm 2.3°$N for this sector (Figure 3c). In contrast, over the Indian Ocean, higher SST warming in the northern subtropics is consistent with the predicted shift of the ITCZ to the north from its current baseline position (Figure 3b). The pattern of SST change in the Indian Ocean resembles a positive Indian Ocean Dipole (IOD) pattern (with more pronounced warming over the northwestern Indian Ocean and less pronounced warming

over the southeastern Indian Ocean), traditionally linked to locally developed Bjerknes feedbacks between SST gradients, and wind and thermocline changes in the basin[47,51,52].

Regarding precipitation shifts over land and changes in monsoonal dynamics, studies have shown a future shift of rainfall occurrence from early to late in the rainy season under climate change for most of the individual monsoons[53-55], while in terms of the sign of total precipitation change, large inter-model spreads are reported over specific regions[55]. Despite the reported uncertainties, generally anticipated changes in regional precipitation are consistent with our results presented herein[56-59]. In particular, over South America, a southward shift of the south Atlantic convergence zone under climate change has been reported in observations and in model projections, due to the strengthening of the south Atlantic subtropical high[57,58]. In contrast, over Africa, recent studies find that intense surface warming over Sahara will deepen the Saharan heat low making the tropical rainbelt migrate seasonally farther to the north, and reside there longer[59,60]. This will alter the rainfall seasonality in the south and will yield to an increased rainfall in the north and an average northward shift of the tropical rainbelt[59]. Lastly, projections show that global warming will most likely cause an increase in the Indian summer monsoon rainfall (see Supporting Figure 3a), accompanied by an enhancement of extreme precipitation events[61,62]. Apart from monsoonal changes, a future zonally asymmetric change of rainfall over land has been recently projected based on model simulations and attributed to plant physiological responses to rising CO_2[63].

Atmospheric energetic constraints

Even though the projected changes in tropical north-south SST gradients are broadly consistent with the revealed zonally contrasting response of the ITCZ, more insight is needed as to why these SST changes occur. Both local and non-local process chains are relevant. For example, the positive IOD pattern in the Indian Ocean has been argued to be a result of the weakening of the Walker circulation locally, but also influenced at its southern margin by the oceanic lateral advection of relatively weak warming signatures from the remote Southern Ocean (see Figure 3a)[47,64-66]. Other non-local mechanisms include extratropics-to-tropics teleconnections, which are usually based on energetic arguments[47,67]. Indeed, in the last two decades, many studies have utilized atmospheric energetic constraints to gain insight into past or future zonal-mean ITCZ shifts[1,5,6,9,12,16,25,67-75]. More recently, similar arguments have been developed[10,76] and used to explain longitudinally-varying ITCZ shifts[76-79]. Here we examine how the zonally contrasting shifts of the ITCZ for the SSP3-7.0 scenario are related to energetic constraints, considering changes in atmospheric energy transport and sector-mean shifts of the energy flux equator.

In response to climate change, models indicate that the net energy input into the atmosphere (see schematic in Figure 4a) will increase in the tropics and decrease at high latitudes 50°-70°, especially over the ocean (see Figure 4b-d for the change in the total energy input, and its partitioning into top-of-atmosphere (TOA) and surface components[80]). Particularly, over the Atlantic Ocean, a pattern of northern atmospheric cooling and southern heating is revealed, which is consistent with a future weakening in the AMOC (i.e. the see-saw response)[22,34,35,37,81-83], while over the Southern Ocean, atmospheric cooling is consistent

with increased heat flux from the atmosphere to the ocean (i.e. ocean heat uptake[64-66]) in response to increasing emissions of greenhouse gases[84]. Moreover, we find an increase in atmospheric heating over the tropics, which is mostly a result of the TOA component of the budget (Figure 4c), and is likely associated with increasing water vapor and anthropogenic greenhouse gases, and cloud radiative effects; i.e., the outgoing longwave radiation escaping to space is reduced in the future (see partitioning of TOA energy change in Supplementary Figure 9c, and [22]). Over land, the effect of decreasing snow and ice albedo (see Supplementary Figure 9b and studies regarding climate change-induced glacier melting over the Himalayas[29,30] and climate change-induced sea ice loss in the Arctic[27,31,85]) and reduction of anthropogenic aerosols[22,26], are partially compensated by increases in OLR cooling (see Supplementary Figure 9c). We find that the net effect of all these processes leads to more energy being added into the atmosphere over land in the northern hemisphere and specifically over Europe, Southeast Asia, North America, and the Arctic (see Figure 4b).

In terms of the zonal mean, the net effect of all these processes leads to an almost zero change in the inter-hemispheric energy asymmetry. Particularly, CMIP6 models predict a change on the order of $\Delta(Q_S - Q_N) = -0.05 \pm 0.21$ PW (Q_S and Q_N refer to the hemisperically integrated atmospheric energy input over the southern and northern hemispheres, respectively) and consistent with the negligible zonal-mean ITCZ shift reported in Table 1. However, when considering the Eurasian sector and the eastern Pacific – Atlantic sector separately, models show a high level of consensus in terms of the sign of the change over each sector (changes are assessed statistically significant; $p < 0.01$). Over the Eurasian sector, most models predict that more energy is added into the northern hemisphere than the southern hemisphere in response to climate change (Figure 4e), which reduces the baseline inter-hemispheric energy asymmetry; i.e. $\Delta(Q_S - Q_N) = -0.24 \pm 0.10$ PW (see Table 1). In contrast, over the eastern Pacific – Atlantic sector, the northern hemisphere atmosphere receives less energy in the future (Figure 4e) probably due to the weakening of the AMOC, which contributes to a northern hemisphere atmospheric cooling; i.e. $\Delta(Q_S - Q_N) = 0.31 \pm 0.16$ PW.

The above results highlight contrasting changes of the inter-hemispheric energy asymmetry to climate change between the two considered sectors. To elucidate how these changes alter the atmospheric energy transport (AET) in the tropics, and thus, the ITCZ, we used a regional energetics framework (see Methods)[10,76], which has only recently been applied to explain sector-mean ITCZ shifts[10,76-79], and to the best of our knowledge, it has not yet been applied to scenarios of future climate change.

Our results show that a robust increase of southward AET occurs over the tropics in the Eurasian sector (see Figure 5a; baseline results for the AET are shown in Supplementary Figure 10), which is consistent with the revealed northward shift of the ITCZ. In contrast, the future cooling over the northern Atlantic Ocean is compensated by changes in the extratropical divergent AET (likely controlled by extratropical eddies; see Figure 4b), but also by a robust increase in the northward energy transport over the tropics of the eastern Pacific – Atlantic sector (see Figure 5a), which is consistent with the revealed southward shift of the ITCZ in this sector. Similarly to the changes in the ITCZ location and in the atmospheric energy input, these results highlight zonally contrasting changes in the

meridional component of the divergent AET, providing more confidence regarding the contrasting ITCZ shifts over these two sectors (future changes in zonal energy fluxes are also consistent with the expected weakening of the Walker circulation[47,51]; compare Figure 5b with Supplementary Figure 10e).

As a final consistency check of the zonally contrasting ITCZ shifts with regional energetics, we evaluate the future shifts of the energy flux equator (a zone where the AET diverges and vanishes[10]; EFE) over the two sectors (see Table 1 and Figures 5c-f). Note that the EFE variability has been shown to be linked with the ITCZ variability, not only in the zonal mean[1,9], but also over large longitudinal sectors, with the ITCZ – EFE link breaking down only over the western and central Pacific[10,86]. Our results show that although CMIP6 models do not predict a robust future EFE shift in the global zonal mean (see Table 1), over the Eurasian sector, the EFE shifts to the north by 0.6 ±0.4°, while over the eastern Pacific – Atlantic sector, the EFE shifts to the south by 1.3 ±1.2° (see also Figure 5c). Both these shifts are statistically significant ($p < 0.01$), and they explain around 40% of the inter-model variance of the projected precipitation change (see Figure 5d). Similar EFE shifts are obtained when using an analytic approximation (see Methods and [10]) to calculate the EFE latitude (see Table 1, Figure 5e and Supplementary Figure 11). Based on this approximation, we find that future EFE shifts are mostly driven by changes in the cross-equatorial AET, and less by changes in the net energy input at the equator (Figure 5f).

Overall, our results show that the zonal differences in the ITCZ response to climate change have a robust statistical and physical link with sector-mean changes in the atmosphere's energy budget. It can also be concluded that CMIP6 models do exhibit consensus over the two considered sectors, highlighting contrasting ITCZ shifts, contrasting changes in the atmospheric energy input, and contrasting EFE shifts. The longitudinally varying response of all these quantities and the corresponding models' consensus have been hidden in the zonal-mean analysis of past work. We have repeated the analysis using 31 CMIP5 models, which yield similar conclusions (see Supplementary Figure 12 and Supplementary Table 2), although the precipitation shift over the Atlantic is less robust, likely due to higher double-ITCZ biases and inter-model spread in CMIP5[87].

Discussion

In this study, the future shifts of the ITCZ and the tropical rainbelt in response to climate change were explored as a function of longitude and season using climate model simulations from CMIP6. We find a zonally contrasting response of the location of the ITCZ, which is robust across different climate models, and different seasons. The sector-wide differences in the ITCZ response are spatially extensive, covering about two thirds of the globe. The contrasting ITCZ response can be summarized as a northward shift over the eastern Africa and Indian Ocean and a southward shift over the eastern Pacific Ocean, South America and the Atlantic Ocean. The latitudinally varying ITCZ response and its robustness have often been masked in previous analysis focusing on zonal-mean ITCZ shifts.

We find that the contrasting ITCZ response is driven by a positive IOD-like SST pattern over the Indian Ocean, and high SST warming near the equator over the eastern Pacific and

Atlantic Oceans that serves as an attractor for a southward shift of the ITCZ from its current position. From an atmospheric energetics perspective, our analysis shows that future climate change induces a zonally contrasting change in the inter-hemispheric heating of the atmosphere, as a result of the combined effect of radiative and dynamical processes both in the atmosphere and ocean. Most models show that future changes consist of increases in atmospheric heating over Eurasia and cooling over the Southern Ocean, which contrasts with atmospheric cooling over the North Atlantic Ocean as a consequence of a projected AMOC weakening[34,35]. These changes in the regional extratropical atmospheric heating induce an increase in the southward energy transport over the tropics of eastern Africa and Indian Ocean (and an northward shift of the EFE), and an increase in the northward energy transport over the tropical eastern Pacific – Atlantic sector (and a southward shift of the EFE), both of which are physically and statistically consistent with the revealed ITCZ response. Our results provide a single theoretical framework for simultaneously explaining anticipated future increases of drought stress in southeastern Africa and Madagascar, intensifying flooding in southern India[56], and greater drought stress in Central America[38] – large hydrological hotspots of global change[88,89] that will have considerable impacts on food security and biodiversity.

We note that although our study establishes consistency between the energetics framework and projected changes in tropical precipitation, only about 40% of the inter-model variance of precipitation change is explained based on energetic arguments. This highlights the important limitations of the energetics framework, already reported in the literature (not only in regional settings[90], but also in the zonal mean[46,91,92]), and the need to further explore mechanisms involving ocean-atmosphere-land coupling at regional scales. To further infer causality, carefully designed idealized climate experiments are needed, as a complement to analyses like this one that attempt to understand mechanisms contributing to robust future changes in the hydrological cycle within and across different Earth system models.

Methods

Probabilistic tracking of the ITCZ.

With regard to regionally tracking the ITCZ, ambiguity exists in the literature as to a precise regional definition of the ITCZ and/or which is the optimal variable/method to use for tracking its position[42]. For example, past studies have variously used surface pressure minimum, surface wind convergence, precipitation maximum, minimum outgoing longwave radiation (OLR) or cloudiness maximum to track the ITCZ[42]. The justification for variously using different variables to track the ITCZ is the assumption that the minima or maxima of these variables collocate with each other (i.e. pressure minima roughly collocate with convergence maxima, etc.). Yet, this assumption may not be true over specific regions or in specific seasons[42], and so, this ambiguity in the regional ITCZ definition is problematic. For the purpose of this study, we have used a multivariate probabilistic framework[43], which tracks the ITCZ over different longitudes and seasons by simultaneously assessing the statistics of multiple variables, and thus increasing the robustness of the tracking approach (see studies[59,93,94] for other similar approaches). In particular, we consider overlapping longitudinal windows, and use the window-mean precipitation and OLR (the two most

common variables in the ITCZ literature) to track the ITCZ. For each window and season, ITCZ points are defined as those which correspond to the maximum (above a certain threshold) joint probability of non-exceedance of the two window-mean variables (note that in cases where precipitation and OLR extrema collocate, the latter definition falls back to simply tracking the points of the extrema, and results would be identical if we were to use either variable on its own). The end product of the method is to provide the probability of every grid point in the tropics to be part of the ITCZ in a longitudinally-explicit manner (see Supplementary Figures 1-2). The resulting probability distribution of ITCZ position is used to compare the climatology and interannual variability of the ITCZ between observations and CMIP6 models during a contemporary base period (1983-2005), as well as to assess future ITCZ changes (defined as the difference between 2075-2100 and the base period).

More specifically, let X denote the variable (e.g. precipitation) used for defining the ITCZ location, and $X_w^{\lambda,t}$ the zonal mean of X within the longitudinal window $[\lambda - w/2,\ \lambda + w/2]$ of width w and during month/season t. The latitudinal distribution of $X_w^{\lambda,t}$ can be obtained from observations or model outputs. For a specified probability of non-exceedance a (tracking threshold), we define $x_{w,a}^{\lambda,t}$ to be the a^{th} quantile of $X_w^{\lambda,t}$, i.e.,

$$F\left(x_{w,a}^{\lambda,t}\right) \equiv \Pr\left[X_w^{\lambda,t} \le x_{w,a}^{\lambda,t}\right] = a$$

where F is the cumulative distribution function (CDF) of $X_w^{\lambda,t}$. We define the random variable $\Phi_{w,a}^{\lambda,t}$ to be the location (in degrees of latitude) at which the ITCZ is most likely to prevail, in longitude λ, and in month/season t. A sample of $\Phi_{w,a}^{\lambda,t}$ may then be the set of latitudinal points $\varphi_{w,a}^{\lambda,t}$ at which the value of $X_w^{\lambda,t}$ exceeds the a^{th} quantile $x_{w,a}^{\lambda,t}$, that is:

$$\begin{aligned} &\{\varphi_{w,a}^{\lambda,t}\}: X_w^{\lambda,t}(\varphi_{w,a}^{\lambda,t}) > x_{w,a}^{\lambda,t} = F^{-1}(a) \qquad \text{or} \\ &\{\varphi_{w,a}^{\lambda,t}\}: F\left(X_w^{\lambda,t}(\varphi_{w,a}^{\lambda,t})\right) > a \end{aligned} \tag{1}$$

In other words, we track the position of ITCZ based on the upper (1 - a)×100% of precipitation in longitude λ and month/season t, which corresponds to the points $\varphi_{w,a}^{\lambda,t}$. When considering the OLR to track the ITCZ, the negative OLR is used, since deep convection associates with minimum (not maximum) OLR. Such an approach is rather computationally efficient and allows the analysis of both the annual-mean location and the intra-annual variability of the ITCZ, simply by obtaining the ITCZ points, $\varphi_{w,a}^{\lambda,t}$, for each calendar month or each season.

When jointly considering multiple (e.g. $M \ge 2$) variables $\mathbf{X} = [X_1, X_2, \ldots, X_M]$ to track the ITCZ (as in this study), the ITCZ points, $\varphi_{w,a}^{\lambda,t}$, also satisfy Equation (1), but F is now the joint CDF of $\mathbf{X}_w^{\lambda,t}$.

Herein, we used a non-exceedance $a = 85\%$ as a tracking threshold (general conclusions have been tested across other thresholds too, to ensure robustness), and we averaged precipitation and OLR over longitudinal windows of width $w = 15°$ (see Supplementary Figures 1-2 for schematics). However, the framework is general and applicable in considering any single variable, and/or jointly distributed multiple variables to define the ITCZ. See [43] for more information.

Atmospheric Energy Budget.

Considering a long enough period (e.g. 1983-2005) so that the energy storage in the atmosphere is negligible[1,95], and assuming that the system is in equilibrium, the atmospheric energy budget is [6,95]:

$$\nabla \cdot \mathbf{F} = R^{\mathrm{TOA}} - O = Q \tag{2}$$

where $\mathbf{F}$ is the vector of vertically-integrated atmospheric moist static energy flux, R^{TOA} is the net energy input at the top of the atmosphere (TOA; i.e. net downward shortwave minus the outgoing longwave radiation) and O is the ocean energy uptake (can be further partitioned into latent/sensible heat and radiative surface components) and represents the heating from the surface (note that the energy storage in the land is negligible on timescales greater than a season[1]). Q is the net energy input into the atmospheric column of unit horizontal area (see schematic in Figure 4a, and Supplementary Figure l0a-b for the distribution of Q in the base period), and Equation (2) states that it is equal to the horizontal divergence of the AET.

Regional Energetics – EFE latitude approximation.

The energy flux $\mathbf{F}$ in Equation (2) can be decomposed into the divergent and rotational components ($\mathbf{F}_\chi$ and $\mathbf{F}_\psi$, respectively), and since the divergence of the rotational component is identically zero (i.e. $\nabla \cdot \mathbf{F}_\psi = 0$), Equation (2) takes the form of Poisson's equation:

$$\nabla \cdot \mathbf{F}_\chi = \nabla^2 \chi = Q \tag{3}$$

where χ is the energy flux potential (an arbitrary scalar function)[10,76], such that its gradient is equal to the divergent component of AET, i.e. $(\partial_x\chi, \partial_y\chi) = \nabla_\chi = \mathbf{F}_\chi = (u_\chi, v_\chi)$. By solving Equation (3), the potential χ (also $\mathbf{F}_\chi$) can be obtained; all derivatives are evaluated in spherical coordinates but written here in Cartesian coordinates for simplicity. The zonal component of the divergent AET is negligible compared to the meridional component outside from the tropics, (i.e. $v_\chi \gg u_\chi$ see Supplementary Figure 10c), while in the tropics, they are of the same magnitude (i.e. both the Walker and Hadley circulations contribute to the divergence of heat; Supplementary Figure 10d-e)[10,76,77].

For a sector with longitudinal boundaries λ_1 and λ_2, the sector-mean position of the EFE (or equivalently of the ITCZ), can be approximated to a first order by meridionally expanding (Taylor series) Equation (3) at the equator[10]:

$$[\varphi_{\mathrm{EFE}}]_{\lambda_1}^{\lambda_2} = -\frac{1}{a}\frac{\left[v_{\chi_0}\right]_{\lambda_1}^{\lambda_2}}{[Q_0]_{\lambda_1}^{\lambda_2} - \frac{1}{\lambda_2-\lambda_1}u_{\chi_0}|_{\lambda_1}^{\lambda_2}} \quad (4)$$

where $[\cdot]_{\lambda_1}^{\lambda_2}$ represents the zonal mean over the sector, subscript "0" represents average values near the equator, and a is Earth's radius.

Definition of ITCZ bias in the models.

The double-ITCZ bias of each CMIP6 model over the eastern Pacific or Atlantic Ocean is defined as the average (over the considered longitudinal sector) difference in the Nov-Apr probability distribution of the ITCZ location between the model and the observations (see Supplementary Figure 6):

$$\Delta P = \frac{1}{\frac{(\lambda_2-\lambda_1)}{r_\lambda}+1}\sum_{\lambda=\lambda_1}^{\lambda_2}\left(\frac{1}{2}\int_{\varphi_1}^{\varphi_2} |\ \Delta\mathrm{PDF}_{\lambda,\varphi}\ |\ d\varphi\right) \quad (5)$$

where $\Delta\mathrm{PDF}_{\lambda,\varphi}$ is the difference in the Nov-Apr probability distribution function (PDF) of the ITCZ location between the model and the observations at latitude φ and longitude λ, and r_λ is the model's longitudinal resolution. For calculating the bias over the Atlantic Ocean, $[\varphi_1, \varphi_2]$ = [15°S, 10°N] and $[\lambda_1, \lambda_2]$ = [310°E, 360°E], while for the eastern Pacific bias, $[\varphi_1, \varphi_2]$ = [10°S, 15°N] and $[\lambda_1, \lambda_2]$ = [200°E, 300°E]. The ITCZ biases of all models are presented in Supplementary Table 1. The average bias (weighted by the longitudinal width of each sector) is also presented.

Correlation significance.

For estimating the $(1 - p)$% intervals corresponding to statistically insignificant linear correlation (for a p-value$p$), we assume a t-distribution: $r_c = \frac{\pm t}{\sqrt{N-2+t^2}}$, where t is the $(1 - p/2)$% quantile of the t-distribution, with d.f. = N-2, and N is the sample size.

Data availability.

The data we use in our analysis are all freely available. We use satellite data (monthly precipitation series on a 0.25° × 0.25° grid[96], and OLR series on a 1° × 1° grid[97], for 1983-2005), and climate model outputs from the sixth phase of the Coupled Model Intercomparison Project[39] (CMIP6); see Supplementary Table 1.

Code availability.

Upon reasonable request, the code that support the findings of this study can be provided by Dr. Antonios Mamalakis (amamalak@rams.colostate.edu).

Supplementary Material

Refer to Web version on PubMed Central for supplementary material.

Acknowledgments

Partial support for this research was provided to EFG, JTR and PS by the National Science Foundation (NSF) under the TRIPODS+ program (DMS-1839336). Moreover, the work of EFG was supported by NSF under the EAGER program (grant ECCS-1839441) and by NASA's Global Precipitation Measurement (GPM) Program (grant 80NSSC19K0684). JTR received support from DOE's Office of Science RUBISCO Science Focus Area and NASA's SMAP, IDS, and CMS programs. JYY and MSP were supported by the NSF Climate and Large-scale Dynamics (CLD) Program under Grants AGS-1833075, AGS-173416 and AGS-1912134. SY was supported by a generous gift to Yale from Todd Sandoz. A research grant from UCI to advance these research ideas is also acknowledged. We thank the climate modeling groups around the world for producing and making their model outputs available. We also acknowledge the help from Dr. Ori Adam and Dr. Benjamin Lintner in discussing parts of this analysis.

References

1. Schneider T, Bischoff T, and Haug GH (2014) Migrations and dynamics of the intertopical convergence zone, Nature, 513, doi:10/nature13636
2. Waliser DE & Gautier C (1993) A satellite-derived climatology of the ITCZ. J. Clim 6, 2162–2174.
3. Trenberth KE, Stepaniak DP, & Caron JM (2000) The global monsoon as seen through the divergent atmospheric circulation. Journal of Climate, 13, 3969–3993. 10.1175/1520-0442(2000)013<3969:TGMAST>2.0.CO;2
4. Adler RF, and Coauthors, 2003: The Version-2 Global Precipitation Climatology Project (GPCP) monthly precipitation analysis (1979–present). J. Hydrometeor, 4, 1147–1167, doi: 10.1175/1525-7541(2003)004,1147:TVGPCP.2.0.CO;2
5. Donohoe A, Marshall J, Ferreira D, and McGee D (2013) The relationship between ITCZ location and cross-equatorial atmospheric heat transport: from the seasonal cycle to the last glacial maximum, Journal of Climate, 26, doi: 10.1175/JCLI-D-12-00467.1
6. Bischoff T and Schneider T (2014) Energetic constraints on the position of the intertropical convergence zone, Journal of Climate, 27, doi: 10.1175/JCLI-D-13-00650.1
7. Berry G, & Reeder MJ (2014). Objective identification of the intertropical convergence zone: Climatology and trends from the ERA-interim. Journal of dimate, 27, 1894–1909. 10.1175/JCLI-D-13-00339.1
8. Wang C and Magnusdottir G (2006) The ITCZ in the central and eastern Pacific on synoptic time scales, Monthly Weather Review, 134, 1405–1421.
9. Adam O, Bischoff T, & Schneider T (2016a). Seasonal and interannual variations of the energy flux equator and ITCZ. Part I: Zonally averaged ITCZ position. Journal of Climate, 29, 3219–3230. 10.1175/JCLI-D-15-0512.1
10. Adam O, Bischoff T, & Schneider T (2016b). Seasonal and interannual variations of the energy flux equator and ITCZ. Part II: Zonally varying shifts of the ITCZ. Journal of Climate, 29, 7281–7293. 10.1175/JCLI-D-15-0710.1
11. Chou C, Tu J-Y, and Tan P-H (2007) Asymmetry of tropical precipitation change under global warming, Geoph. Res. Let, 34, doi: 10.1029/2007GL030327
12. Sachs JP, Sachse D, Smittenberg RH, Zhang Z, Battisti DS, and Golubic S (2009) Southward movement of the Pacific intertropical convergence zone AD 1400–1850, Nature Geoscience, 2, doi: 10.1038/NGEO554
13. Cai W et al. (2012) More extreme swings of the South Pacific convergence zone due to greenhouse warming. Nature 488, 365–369. [PubMed: 22895343]
14. Broecker WS, and Putnam AE (2013) Hydrologic impacts of past shifts of Earth's thermal equator offer insight into those to be produced by fossil fuel CO_2, PNAS, 110(42)
15. Arbuszewski JA, deMenocal PB, Cléroux C, Bradtmiller L, Mix A (2013) Meridional shifts of the Atlantic intertropical convergence zone since the Last Glacial Maximum, Nature Geoscience, 6, doi: 10.1038/NGEO1961
16. Hwang Y-T, Frierson DMW, and Kang SM (2013) Anthropogenic sulfate aerosol and the southward shift of tropical precipitation in the late 20th century, Geoph. Res. Lett, 40, doi: 10.1002/grl.50502

17. Lau WKM, and Kim K-M (2015), Robust Hadley circulation changes and increasing global dryness due to CO2 warming from CMIP5 model projections, Proc. Natl. Acad. Sci. U.S.A, 112, 3630–3635. [PubMed: 25713344]
18. Allen RJ (2015), A 21st century northward tropical precipitation shift caused by future anthropogenic aerosol reductions, J. Geophys. Res. Atmos, 120, 9087–9102, doi: 10.1002/2015JD023623.
19. Allen RJ, Evan AT, Booth BBB (2015) Interhemispheric aerosol radiative forcing and tropical precipitation shifts during the late twentieth century, Journal of Climate, 28, doi: 10.1175/JCLI-D-15-0148.1
20. Byrne MP, and Schneider T (2016), Narrowing of the ITCZ in a warming climate: Physical mechanisms, Geophys.Res. Lett, 43, 11,350–11,357, doi:10.1002/2016GL070396.
21. Chung E-S and Soden BJ (2017) Hemispheric climate shifts driven by anthropogenic aerosol-cloud interactions, Nature Geoscience, 10, doi: 10.1038/NGEO2988
22. McFarlane AA, and Frierson DMW (2017), The role of ocean fluxes and radiative forcings in determining tropical rainfall shifts in RCP8.5 simulations, Geophys. Res. Lett, 44, 8656–8664, doi:10.1002/2017GL074473.
23. Bony S et al., (2015) Clouds, circulation and climate sensitivity, Nature Geoscience, 8, 261–268.
24. Cox PM, Harris PP, Huntingford C, Betts RA, Collins M, Jones CD, Jupp TE, Marengo JA, and Nobre CA. (2008) Increasing risk of Amazonian drought due to decreasing aerosol pollution, Nature 453, no. 7192: 212. [PubMed: 18464740]
25. Rotstayn L, Collier M, and Luo J (2015) Effects of declining aerosols on projections of zonally averaged tropical precipitation. Environ. Res, 10, 044018.
26. Lamarque JM, Kyle G, Meinshausen M, Riahi K, Smith S, van Vuuren D, Conley A, and Vitt F (2011), Global and regional evolution of shortlived radiatively-active gases and aerosols in the representative concentration pathways, Clim. Change, 109, 191–212.
27. Serreze MC, and Barry RG, (2011) Processes and impacts of arctic amplification: A research synthesis. Global Planet. Change, 77, 85–96, doi:10.1016/j.gloplacha.2011.03.004.
28. Labe Z, Magnusdottir G and Stern H (2018) Variability of Arctic sea ice thickness using PIOMAS and the CESM large ensemble, J. Climate, 31, 3233–3247.
29. Immerzeel WW, Pellicciotti F and Bierkens MFP (2013) Rising river flows throughout the twenty-first century in two Himalayan glacierized watersheds, Nat. Geosci, 6, 742–5
30. Chaturvedi RK, Kulkarni A, Karyakarte Y, Joshi J and Bala G (2014) Glacial mass balance changes in the Karakoram and Himalaya based on CMIP5 multi-model climate projections, Clim. Change, 123, 315–28
31. Tomas RA, Deser C, and Sun L, 2016: The role of ocean heat transport in the global climate response to projected Arctic sea ice loss. J. Climate, 29, 6841–6859, doi: 10.1175/JCLI-D-15-0651.1.
32. Weaver AJ et al. (2012) Stability of the Atlantic meridional overturning circulation: A model intercomparison. Geophys. Res. Lett, 39, L20709.
33. Cheng W, Chiang JCH, and Zhang D (2013) Atlantic meridional overturning circulation (AMOC) in CMIP5 models: RCP and historical simulations. J. Climate, 26, 7187–7197.
34. Rahmstorf S, Box JE, Feulner G, Mann ME, Robinson A, Rutherford S, & Schaffernicht EJ (2015). Exceptional twentieth-century slowdown in Atlantic Ocean overturning circulation. Nature Climate Change, 5(5), 475–480. 10.1038/nclimate2554
35. Weijer W, Cheng W, Garuba OA, Hu A, & Nadiga BT (2020) CMIP6 models predict significant 21st century decline of the Atlantic Meridional Overturning Circulation, Geophys. Res. Lett, 47, e2019GL086075. 10.1029/2019GL086075
36. Caesar L, Rahmstorf S, Robinson A, Feulner G, & Saba V (2018). Observed fingerprint of a weakening Atlantic Ocean overturning circulation. Nature, 556(7700), 191–196. 10.1038/s41586-018-0006-5 [PubMed: 29643485]
37. Zhang R and Delworth TL (2005) Simulated topical response to a substantial weakening of the Atlantic thermohaline circulation, Journal of Climate, 18, 1853–1860

38. Chen Y, Langenbrunner B, & Randerson JT (2018). Future drying in Central America and northern South America linked with Atlantic meridional overturning circulation. Geophysical Research Letters, 45, 9226–9235. 10.1029/2018GL077953
39. Eyring et al. (2016) An overview of the Coupled Model Intercomparison Project Phase 6 (CMIP6) experimental design and organization, Geosci. Model Dev, 9, 1937–1958,, doi: 10.5194/gmd-9-1937-2016
40. O'Neill BC et al. (2017) The roads ahead: Narratives for shared socioeconomic pathways describing world futures in the first 21st century, Global Environmental Change, 42, 169–180.
41. Van Vuuren DP, et al., (2011) Representative concentration pathways: An overview, Climatic Change, 109, 5–31, doi:10.1007/s10584-011-0148-z
42. Nicholson SE (2018) The ITCZ and the seasonal cycle over equatorial Africa, BAMS, 99, 337–348.
43. Mamalakis A, & Foufoula-Georgiou E (2018). A multivariate probabilistic framework for tracking the intertropical convergence zone: Analysis of recent climatology and past trends. Geophysical Research Letters, 45. 10.1029/2018GL079865
44. Byrne MP, Pendergrass AG, Rapp AD, Wodzicki KR (2018) Response of the Intertropical Convergence Zone to Climate Change: Location, Width, and Strength, Current Climate Change Reports, 4, 355–370. [PubMed: 30931244]
45. Pauluis O, (2004) Boundary Layer Dynamics and Cross-Equatorial Hadley Circulation, Journal of the Atmospheric Sciences, 61, 1161–1173.
46. Wei H-H, & Bordoni S (2018) Energetic constraints on the ITCZ position in idealized simulations with a seasonal cycle. Journal of Advances in Modeling Earth Systems, 10, 1708–1725. 10.1029/2018MS001313
47. Xie S-P et al. (2010) Global warming pattern formation: sea surface temperature and rainfall, J. Clim 23, 966–986.
48. Dutheil C, et al., (2019) Impact of temperature biases on climate change projections of the South Pacific Convergence Zone, Clim. Dyn, 10.1007/s00382-019-04692-6.
49. Kang SM and Held IM (2012) Tropical precipitation, SSTs and the surface energy budget: a zonally symmetric perspective, Clim. Dyn, 38, 1917–1924.
50. Xiang B, Zhao M, Ming Y, Yu W, and Kang SM (2018) Contrasting Impacts of Radiative Forcing in the Southern Ocean versus Southern Tropics on ITCZ Position and Energy Transport in One GFDL Climate Model, J. Clim 31, 5609–5628.
51. Vecchi GA and Soden BJ (2007) Global Warming and the Weakening of the Tropical Circulation, J. Clim, 20, 4316–4340.
52. Saji NH, Goswami BN, Vinayachandran PN, and Yamagata T (1999) A dipole mode in the tropical Indian Ocean. Nature, 401, 360–363. [PubMed: 16862108]
53. Seth A, Rauscher SA, Rojas M et al. (2011) Enhanced spring convective barrier for monsoons in a warmer world?, Climatic Change, 104, 403–414. 10.1007/s10584-010-9973-8
54. Seth A, Rauscher SA, Biasutti M, Giannini A, Camargo SJ, and Rojas M (2013) CMIP5 Projected Changes in the Annual Cycle of Precipitation in Monsoon Regions, J. Climate, 26, 7328–7351, 10.1175/JCLI-D-12-00726.1.
55. Rodríguez-Fonseca B, and Coauthors (2015) Variability and Predictability of West African Droughts: A Review on the Role of Sea Surface Temperature Anomalies, J. Climate, 28, 4034–4060, 10.1175/JCLI-D-14-00130.1.
56. D'Agostino R, Bader J, Bordoni S, Ferreira D, & Jungclaus J (2019). Northern Hemisphere monsoon response to mid-Holocene orbital forcing and greenhouse gas-induced global warming. Geophysical Research Letters, 46, 1591–601. 10.1029/2018GL081589
57. Pascale S, Carvalho LMV, Adams DK, Castro CL, & Cavalcanti IFA (2019), Current and Future Variations of the Monsoons of the Americas in a Warming Climate. Current Climate Change Reports, 5(3), 125–144. 10.1007/s40641-019-00135-w
58. Zilli MT, Carvalho LMV & Lintner BR (2019) The poleward shift of South Atlantic Convergence Zone in recent decades, Clim Dyn, 52, 2545–2563. 10.1007/s00382-018-4277-1
59. Dunning CM, Black E, and Allan RP, (2018) Later Wet Seasons with More Intense Rainfall over Africa under Future Climate Change. J. Climate, 31, 9719–9738, 10.1175/JCLI-D-18-0102.1.

60. Cook KH, Vizy EK (2012) Impact of climate change on mid-twenty-first century growing seasons in Africa. Clim Dyn 39, 2937–2955, 10.1007/s00382-012-1324-1
61. Menon A, Levermann A, Schewe J, Lehmann J & Frieler K (2013) Consistent increase in Indian monsoon rainfall and its variability across CMIP-5 models, Earth. Sys. Dyn, 4, 287–300.
62. Sharmila S, Joseph S, Sahai AK, Abhilash S & Chattopadhyay R (2015) Future projection of Indian summer monsoon variability under climate change scenario: An assessment from CMIP5 climate models, Global and Planetary Change, 124, 62–78.
63. Kooperman GJ, Chen Y, Hoffman FM, Koven CD, Lindsay K, et al. 2018. Forest response to rising CO2 drives zonally asymmetric rainfall change over tropical land. Nat. Clim. Change, 8: 434–40.
64. Hwang Y-T, Xie S-P, Deser C, and Kang SM (2017), Connecting tropical climate change with Southern Ocean heat uptake, Geophys. Res. Lett, 44, 9449–9457, doi:10.1002/2017GL074972.
65. Frölicher TL, Sarmiento JL, Paynter DJ, Dunne JP, Krasting JP, and Winton M (2015), Dominance of the Southern Ocean in anthropogenic carbon and heat uptake in CMIP5 models, J. Clim, 28, 862–886.
66. Roemmich D, Church J, Gilson J, Monselesan D, Sutton P, and Wjiffels S (2015), Unabated planetary warming and its ocean structure since 2006, Nat. Clim. Change, 5, 240–254.
67. Kang SM, Held IM, Frierson DMW, & Zhao M (2008). The response of the ITCZ to extratropical thermal forcing: Idealized slab-ocean experiments with a GCM. Journal of Climate, 21, 3521–3532. 10.1175/2007JCLI2146.1
68. Moreno-Chamarro E, Marshall J, and Delworth TL, (2020) Linking ITCZ migrations to the AMOC and North Atlantic/Pacific SST decadal variability, J. Climate, 33, 893–905.
69. Haywood JM, Jones A, Bellouin N, and Stephenson D, (2013) Asymmetric forcing from stratospheric aerosols impacts Sahelian rainfall, Nat. Climate Change, 3, 660–665, doi:10.1038/nclimate1857.
70. Chiang JCH, & Bitz CM (2005). Influence of high latitude ice cover on the marine intertropical convergence zone. Climate Dynamics, 25, 477–496. 10.1007/s00382-005-0040-5
71. Broccoli AJ, Dahl KA, & Stouffer RJ (2006). Response of the ITCZ to Northern Hemisphere cooling. Geophysical Research Letters, 33, L01702. 10.1029/2005GL024546
72. Frierson DMW, and Hwang Y-T (2012), Extratropical influence on ITCZ shifts in slab ocean simulations of global warming, J. Clim, 25, 720–733.
73. Hwang Y, and Frierson D (2013) Link between the double-intertropical convergence zone problem and cloud biases over the Southern Ocean. Proc. Natl. Acad. Sci. USA, 110, 4935–4940. [PubMed: 23493552]
74. Green B, and Marshall J (2017) Coupling of trade winds with ocean circulation damps ITCZ shifts. J. Climate, 30, 4395–4411.
75. Yu S and Pritchard MS, 2019: A strong role for the AMOC in partitioning global energy transport and shifting ITCZ position in response to latitudinally discrete solar forcing in the CESM1.2., J. Climate, 10.1175/JCLI-D-18-0360.1
76. Boos WR & Korty RL Regional energy budget control of the intertropical convergence zone and application to mid-Holocene rainfall. Nat. Geosci 9, 892–897 (2016).
77. Adam O, Schneider T & Brient F (2018) Regional and seasonal variations of the double-ITCZ bias in CMIP 5 models, Clim. Dyn, 51 (101). 10.1007/s00382-017-3909-1
78. Adam O, Schneider T, Enzel Y and Quade J (2019) Both differential and equatorial heating contributed to African monsoon variations during mid-Holocene, Earth and Planetary Science Letters, 522, 20–29.
79. Lintner B, and Boos W (2019) Using atmospheric energy transport to quantitatively constrain South Pacific Convergence Zone shifts during ENSO, J. Climate, 32, 1839–1855.
80. Feldl N and Bordoni S (2016) Characterizing the Hadley circulation through regional climate feedbacks, J. Clim, 29, 613–622.
81. Rahmstorf S, (2002) Ocean circulation and climate during the past 120,000 years, Nature, 419, 207–214. [PubMed: 12226675]
82. Cheng W, Bitz CM, and Chiang JCH (2007), Adjustment of the global climate system to abrupt changes in the Atlantic meridional overturning circulation, in Ocean Circulation: Mechanisms and

Impacts, Geophys. Monogr. Ser, vol. 173, edited by Schmittner A, Chiang J, and Hemming S, pp. 295–314, AGU, Washington, D. C.

83. Drijfhout S, van Oldenborgh GJ & Cimatoribus A (2012) Is a decline of AMOC causing the warming hole above the North Atlantic in observed and modeled warming patterns? J. Clim 25, 8373–8379.
84. Swart NC, Gille ST, Fyfe JC, and Gillet NP (2018) Recent Southern Ocean warming and freshening driven by greenhouse gas emissions and ozone depletion, Nature Geoscience, 11, 836–841.
85. Deser C, Tomas RA, and Sun L, (2015) The role of ocean-atmosphere coupling in the zonal-mean atmospheric response to Arctic Sea ice loss. Journal of Climate, 28, 2168–2186, doi: 10.1175/JCLI-D-14-00325.1.
86. Wei H-H, & Bordoni S (2020) Energetic Constraints on the intertropical convergence zone position in the observed seasonal cycle from Modern-Era Retrospective analysis for Research and Applications, Version 2 (MERRA-2). Geophysical Research Letters, 47, e2020GL088506. 10.1029/2020GL088506
87. Tian B, & Dong X (2020) The double-ITCZ Bias in CMIP3, CMIP5 and CMIP6 models based on annual mean precipitation, Geophysical Research Letters, 47, e2020GL087232. 10.1029/2020GL087232
88. Diffenbaugh NS, & Giorgi F (2012). Climate change hotspots in the CMIP5 global climate model ensemble. Climatic Change, 114(3–4), 813–822. 10.1007/s10584-012-0570-x [PubMed: 24014154]
89. Xu L, Wang A, Wang D, & Wang H (2019). Hot spots of climate extremes in the future. Journal of Geophysical Research: Atmospheres, 124, 3035–3049. 10.1029/2018JD029980
90. Hill SA (2019) Theories for Past and Future Monsoon Rainfall Changes. Curr Clim Change Rep, 5, 160–171. 10.1007/s40641-019-00137-8
91. Kang SM, Shin Y & Xie S (2018) Extratropical forcing and tropical rainfall distribution: energetics framework and ocean Ekman advection. npj Clim Atmos Sci, 1, 20172. 10.1038/s41612-017-0004-6
92. Biasutti M, and Voigt A, (2020) Seasonal and CO_2-Induced Shifts of the ITCZ: Testing Energetic Controls in Idealized Simulations with Comprehensive Models. J. Climate, 33, 2853–2870, 10.1175/JCLI-D-19-0602.1.

References

93. Shonk JKP, Guilyardi E, Toniazzo T et al. (2018) Identifying causes of Western Pacific ITCZ drift in ECMWF System 4 hindcasts. Clim Dyn, 50, 939–954. 10.1007/s00382-017-3650-9
94. Bain CL, et al. (2011) Detecting the ITCZ in instantaneous satellite data using spatiotemporal statistical modeling: ITCZ climatology in the east Pacific, J. Climate, 24, doi: 10.1175/2010JCLI3716.1
95. Hartmann DL (2016) Global Physical Climatology (Elsevier, Amsterdam), 2nd Ed.
96. Ashouri H, Hsu KL, Sorooshian S, Braithwaite DK, Knapp KR, Cecil LD, Nelson BR, and Prat OP (2015) PERSIANN-CDR: Daily Precipitation Climate Studies Data Record from Multisatellite Observations for /Hydrological and Climate Studies, Bull. Amer. Meteor. Soc, 96, 69–83, doi: 10.1175/BAMS-D-13-00068.1.
97. Lee H-T (2014). Climate algorithm theoretical basis document (C-ATBD): Outgoing longwave radiation (OLR)—Daily. NOAA's Climate Data Record (CDR) Program, CDRP-ATBD-0526 (46 pp.)

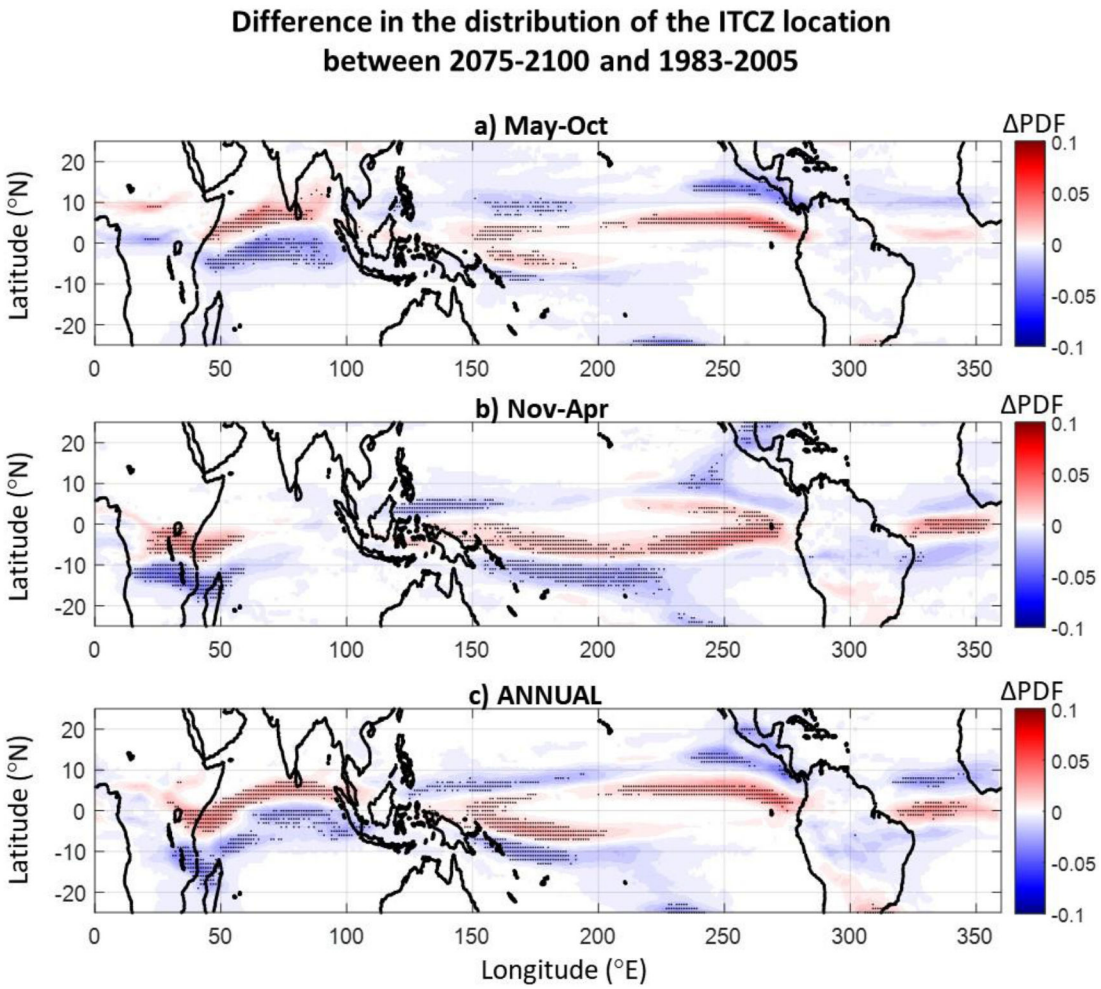

Figure 1: Future changes in the location of the ITCZ in response to climate change, as projected by CMIP6 models.

a) Difference in the probability density function (ΔPDF) of the location of the ITCZ in May-Oct between 2075-2100 and 1983-2005. In each period, the location of the ITCZ is defined by tracking the location of maximum precipitation and minimum outgoing longwave radiation (OLR) in overlapping longitudinal windows (we use the joint statistics of the two variables; see Supplementary Figures 1-2 and Methods). b) Same as in (a), but for Nov-Apr. c) Same as in (a), but the changes in the annual distribution are shown. In all plots, the multi-model mean across 27 CMIP6 models is presented, while stippling indicates agreement (in the sign of the change) in more than ¾ of the models considered. Results indicate a robust northward ITCZ shift over eastern Africa and Indian Ocean and a southward ITCZ shift over eastern Pacific and Atlantic Oceans.

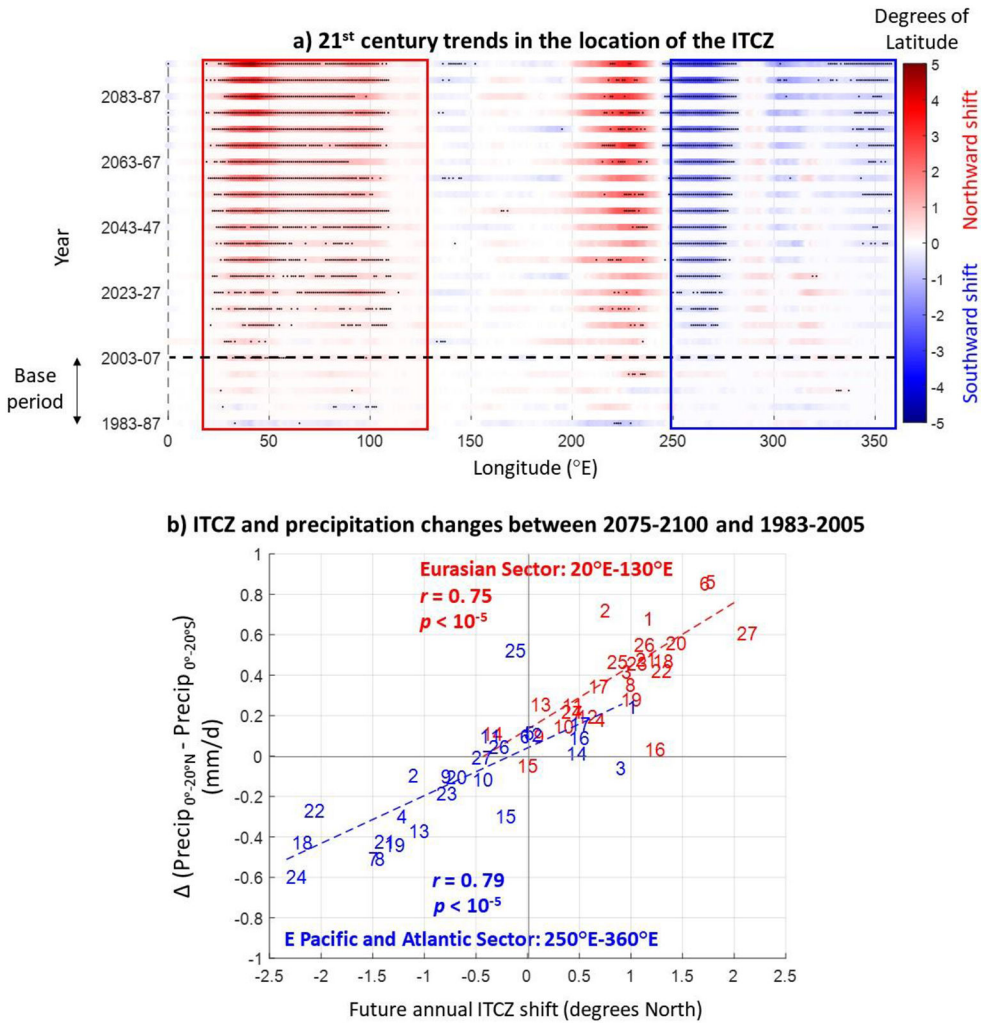

Figure 2: 21st century series of ITCZ location as projected by CMIP6 models.

a) Series of the 5yr-mean ITCZ location relative to the base period as a function of longitude (positive values imply a northward shift). The multi-model mean across 27 CMIP6 models is presented, while stippling indicates agreement (in the sign of the change) in more than ¾ of the models considered. b) Scatter plot of the projected annual ITCZ shift (horizontal axis) and change of tropical precipitation asymmetry (vertical axis) between the periods 2075-2100 and 1983-2005, using all 27 CMIP6 models zonally averaged over the Eurasian sector (20°E-130°E; red color) and the eastern Pacific – Atlantic sector (250°E-360°E; blue color). Each model is labeled according to Supplementary Table 1. For models with multiple runs, the average shift across all runs is presented. Based on either index (ITCZ shift or precipitation asymmetry), a robust contrasting ITCZ response between the two sectors is visible, whereby the ITCZ is projected to shift northward in the Eurasian sector and southward in eastern Pacific – Atlantic sector. The northward ITCZ shift shown in panel (a) over 200°E-250°E, is an artifact coming from the negative pattern at 25°S shown in Figure 1c, which dominates the change of the mean of the PDF in these longitudes.

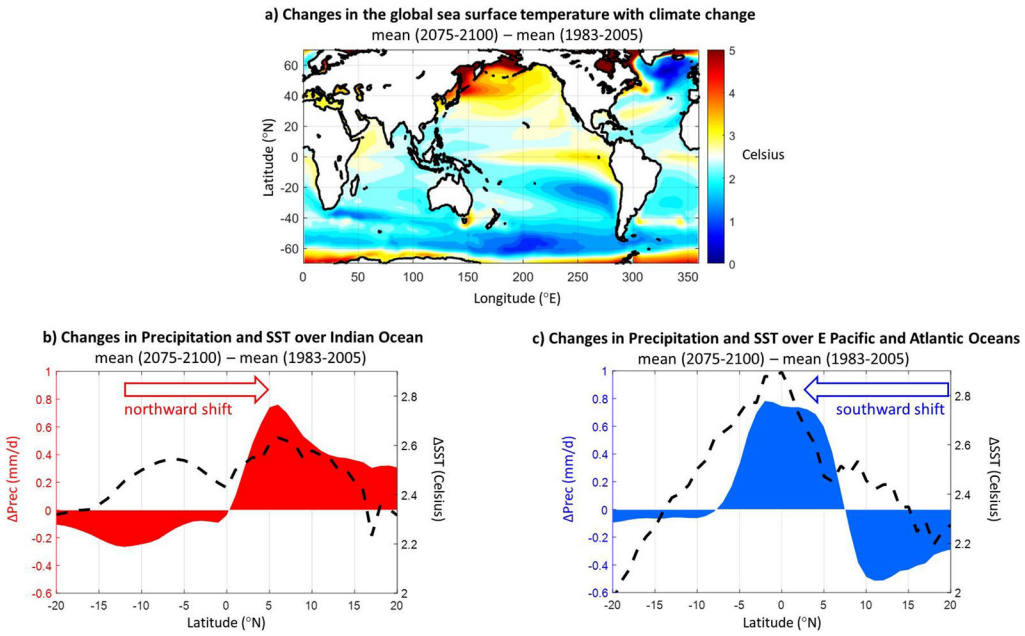

Figure 3: Future changes in sea surface temperature and precipitation in response to climate change, as projected by CMIP6 models.

a) Global changes in sea surface temperature (SST) between future 2075-2100 and base period 1983-2005. b) Zonal mean over the Indian Ocean (50°E-100°E) of the changes of precipitation (in mm/d) and SST (in Celsius). c) Same as in (b), but for the eastern Pacific and Atlantic Oceans (250°E-360°E); land changes are not considered in the zonal mean. All results refer to the multi-model mean across 27 CMIP6 models.

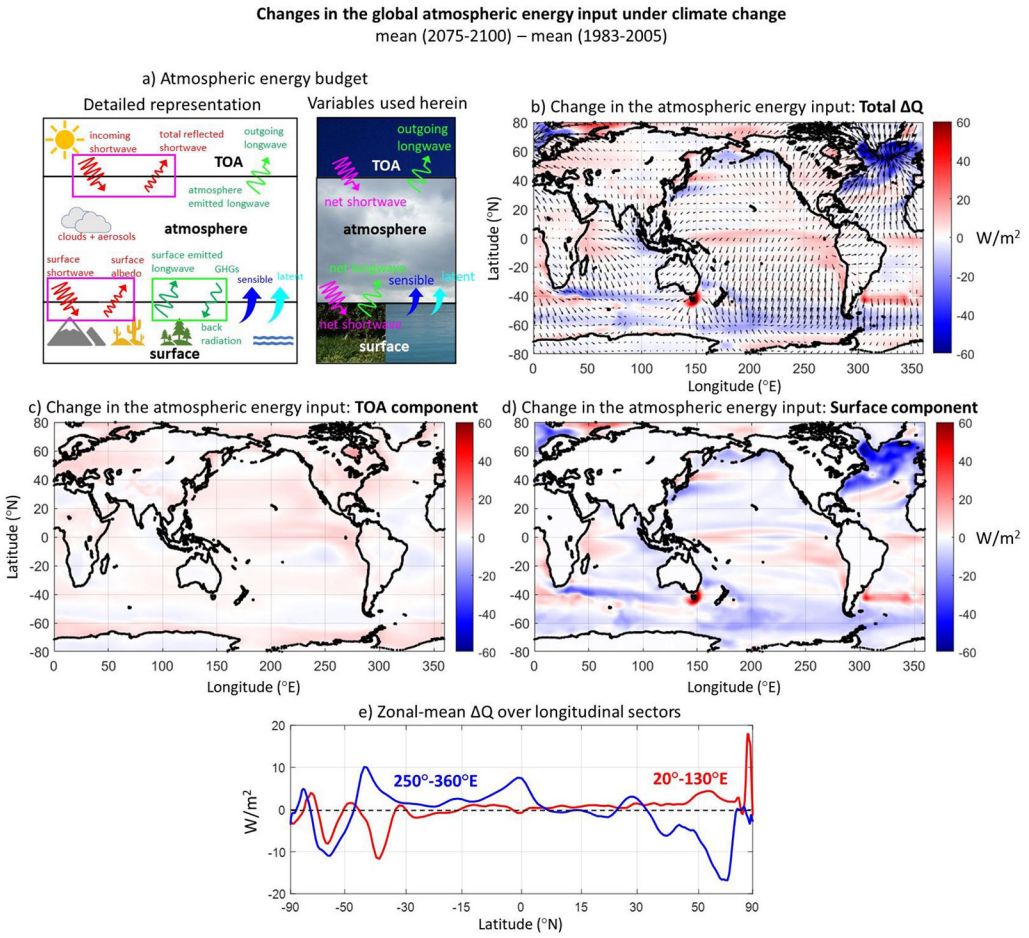

Figure 4: Future changes in the atmospheric energy input in response to climate change, as projected by CMIP6 models.

a) Graphic representation of the atmospheric energy budget. b) Difference of the average energy atmospheric input between 2075-2100 and 1983-2005 periods (shading), while vectors show the change in the divergent component of the atmospheric energy transport; vectors are on the order of 10^7 W/m (see Figure 5 for specific values). c) Same as in (b), but only the top of the atmosphere (TOA) component is shown. d) Same as in (b), but only the surface component is shown. This panel highlights the contribution of the ocean to the future atmospheric heating/cooling. e) Zonal mean of (b) over the Eurasian sector (20°E-130°E; red curve) and the eastern Pacific – Atlantic sector (250°E-360°E; blue curve). The horizontal axis is scaled as $\sin(\varphi)$[72]. In all plots, the multi-model mean across 27 CMIP6 models is presented. Results show that under global climate change, more energy is added in the atmosphere over the northern hemisphere than the southern hemisphere in the Eurasian sector, while the opposite is true in the eastern Pacific – Atlantic sector.

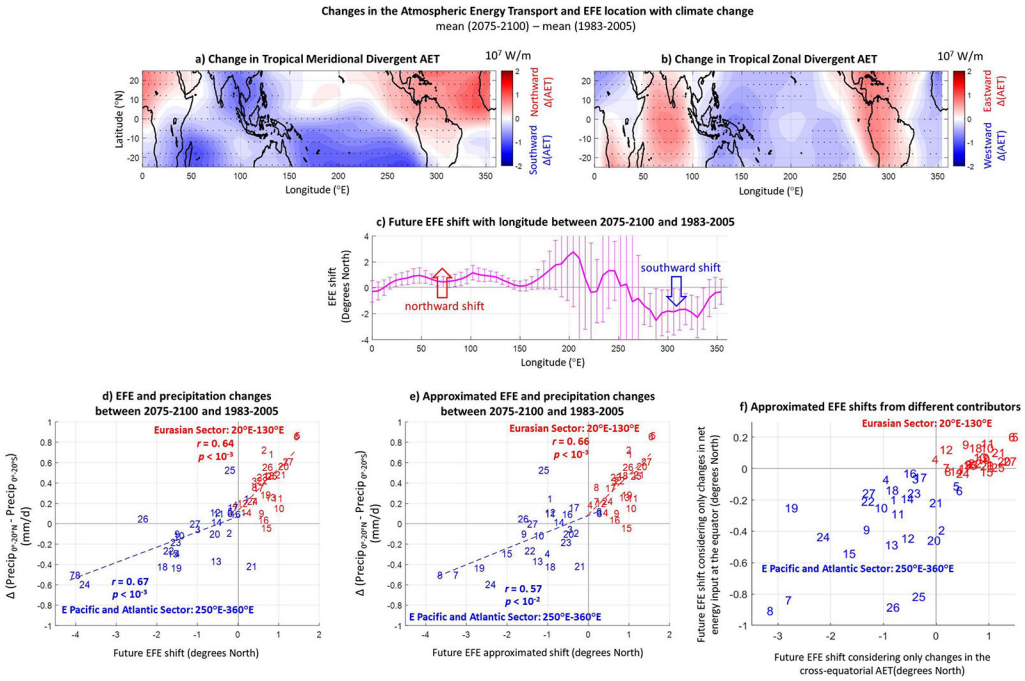

Figure 5: Future changes in the atmospheric energy transport (AET) over the tropics and the energy flux equator (EFE) in response to climate change, as projected by CMIP6 models.

a) Change in the divergent meridional component of the AET over the tropics between 2075-2100 and 1983-2005. The multi-model mean across 27 CMIP6 models is presented, while stippling indicates agreement (in the sign of the change) in more than ¾ of the models considered. b) Same as in (a), but for the divergent zonal component. c) Future EFE shift as a function of longitude. EFE is tracked by the latitude where the divergent meridional AET diverges and vanishes. The magenta curve shows the multi-model mean, while the error bars show the inter-model spread (± st. dev.). d) Change in the precipitation asymmetry (between 2075-2100 and 1983-2005) as a function of the EFE shift, using all 27 CMIP6 models zonally averaged over the Eurasian sector (20°E-130°E; red color) and the eastern Pacific – Atlantic sector (250°E-360°E; blue color). Each model is labeled according to Supplementary Table 1. For models with multiple runs, the average shift across all runs is presented. e) Same as in (d), but the EFE shifts are approximated using the analytic expression in Equation (4); see Methods. f) The EFE shifts in (e) are decomposed into shifts that consider changes only in the cross-equatorial AET (horizontal axis) or only in net energy input at the equator (vertical axis). Results show that with climate change, the future state of the atmospheric energy transport will be characterized by an increased southward transport (divergent component) over the tropical Eurasian sector, which implies a northward shift of EFE, and it is statistically consistent with a northward shift of the ITCZ. The opposite (i.e. increased northward energy transport and southward shift of EFE) is true in the eastern Pacific – Atlantic sector. Also, future EFE shifts are shown to be dominated by changes in cross-equatorial AET.

Table 1:

Mean and standard deviation of the future ITCZ and EFE shifts (2075-2100 minus 1983-2005, positive values indicate northward movement) and changes of the inter-hemispheric energetic asymmetry over different longitudinal sectors, as obtained from 27 CMIP6 model outputs. The baseline values (i.e. referring to 1983-2005) are also provided. Values with **bold** font correspond to a multi-model mean which is statistically distinguishable from zero, based on the *t*-test ($p < 0.01$). It is shown that there is a robust consensus across models regarding future changes in the Eurasian and eastern Pacific – Atlantic sectors, but such a consensus is not apparent in the global zonal mean. Note for example that in the sector-mean analysis, the inter-model variability (i.e. st. deviation) in future changes is either smaller or of the same magnitude with the multi-model mean, while in the global zonal-mean analysis the inter-model variability is in all cases 2 to 4 times larger than the multi-model mean.

27 CMIP6 Models		**Global zonal mean**	**Eurasian Sector [20°E-130°E]**	**E Pacific – Atlantic Sector [250°E-360°E]**
ITCZ latitude (°N)	Base Period	**3.6 ±2.0**	**−1.0 ±1.1**	**4.1 ±2.3**
	Future Shift	−0.5 ±1.2	**0.8 ±0.6**	**−0.7 ±0.9**
Q_S - Q_N (PW)	Base Period	−0.03 ±0.37	**0.93 ±0.21**	**−0.96 ±0.23**
	Future Change	−0.05 ±0.21	**−0.24 ±0.10**	**0.31 ±0.16**
EFE latitude (°N)	Base Period	−0.3 ±1.1	**−3.5 ±0.8**	**4.4 ±2.2**
	Future Shift	0.0 ±0.6	**0.6 ±0.4**	**−1.3 ±1.2**
EFE latitude approximation[10] (°N)	Base Period	−0.4 ±0.8	**−3.3 ±0.9**	**4.5 ±1.7**
	Future Shift	0.2 ±0.5	**0.7 ±0.4**	**−1.3 ±1.0**